ORGANOMETALLICS

Article

pubs.acs.org/Organometallics

Improved Catalytic Activity of Ruthenium–Arene Complexes in the Reduction of NAD$^+$

Joan J. Soldevila-Barreda,[†,§] Pieter C. A. Bruijnincx,[‡,§] Abraha Habtemariam,[†] Guy J. Clarkson,[†] Robert J. Deeth,[†] and Peter J. Sadler*[,†]

[†]Department of Chemistry, University of Warwick, Gibbet Hill Road, Coventry CV4 7AL, U.K.

[‡]Debye Institute of Nanomaterials Science, Inorganic Chemistry & Catalysis, Utrecht University, Universiteitsweg 99, 3584 CG Utrecht, The Netherlands

S Supporting Information

ABSTRACT: A series of neutral Ru^{II} half-sandwich complexes of the type [(η^6-arene)Ru(N,N′)Cl] where the arene is *para*-cymene (*p*-cym), hexamethylbenzene (hmb), biphenyl (bip), or benzene (bn) and N,N′ is *N*-(2-aminoethyl)-4-(trifluoromethyl)benzenesulfonamide (TfEn), *N*-(2-aminoethyl)-4-toluenesulfonamide (TsEn), or *N*-(2-aminoethyl)-methylenesulfonamide (MsEn) were synthesized and characterized. X-ray crystal structures of [(*p*-cym)Ru(MsEn)Cl] (**1**), [(hmb)Ru(TsEn)Cl] (**5**), [(hmb)Ru(TfEn)Cl] (**6**), [(bip)Ru(MsEn)Cl] (**7**), and [(bip)Ru(TsEn)Cl] (**8**) have been determined. The complexes can regioselectively catalyze the transfer hydrogenation of NAD$^+$ to give 1,4-NADH in the presence of formate. The turnover frequencies (TOF) when the arene is varied decrease in the order bn > bip > *p*-cym > hmb for complexes with the same N,N′ chelating ligand. The TOF decreased with variation in the N,N′ chelating ligand in the order TfEn > TsEn > MsEn for a given arene. [(bn)Ru(TfEn)Cl] (**12**) was the most active, with a TOF of 10.4 h^{-1}. The effects of NAD$^+$ and formate concentration on the reaction rates were determined for [(*p*-cym)Ru(TsEn)Cl] (**2**). Isotope studies implicated the formation of [(arene)Ru(N,N′)(H)] as the rate-limiting step. The coordination of formate and subsequent CO_2 elimination to generate the hydride were modeled computationally by density functional theory (DFT). CO_2 elimination occurs via a two-step process with the coordinated formate first twisting to present its hydrogen toward the metal center. The computed barriers for CO_2 release for arene = benzene follow the order MsEn > TsEn > TfEn, and for the MsEn system the barrier followed bn < hmb, both consistent with the observed rates. The effect of methanol on transfer hydrogenation rates in aqueous solution was investigated. A study of pH dependence of the reaction in D_2O gave the optimum pH* as 7.2 with a TOF of 1.58 h^{-1} for **2**. The series of compounds reported here show an improvement in the catalytic activity by an order of magnitude compared to the ethylenediamine analogues.

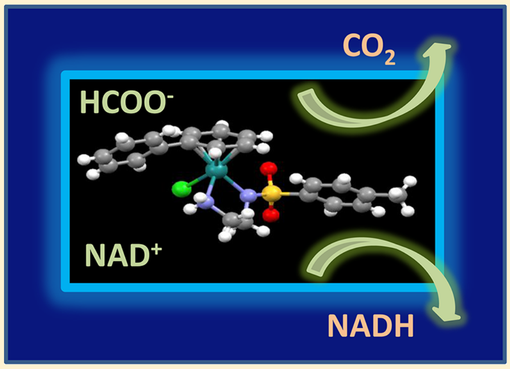

■ INTRODUCTION

The coenzyme nicotinamide adenine dinucleotide (NAD$^+$) and its reduced form 1,4-NADH have crucial roles in many cellular metabolic processes such as regulation of energy metabolism, antioxidative function, DNA repair and transcription, immunological functions, and cell death.[1] The coenzymes are involved in many other processes, acting as substrates and cofactors for enzymes such as NAD$^+$ ligases, oxidoreductases, polymerases, and deacetylases involved in biosynthesis.

The coenzymes NAD$^+$/NADH have been studied intensively during the past few years. It has been demonstrated that changes in metabolism result in fluctuations in the ratio NAD$^+$/NADH or, conversely, changes in the ratio can produce metabolic changes.[2] In some cases alterations in the cellular redox status have been shown to play an important role in cell death, and therefore the coenzymes have become possible drug targets for chronic or autoimmune diseases such as Parkinson's, hepatitis C, diabetic vascular dysfunction, hyperglycemia, and cancer.[3]

The concentration of NAD$^+$ and the ratio NAD$^+$/NADH have been shown to be very important for cancer cells. On the one hand, due to their active metabolism, cancer cells generate high levels of oxidizing species and, therefore, they are under constant oxidative stress.[4] This makes cancer cells more dependent on redox regulatory systems and more sensitive to variations in the NAD$^+$/NADH ratio. On the other hand, NAD$^+$ is required as a substrate for many enzymatic reactions such as ADP-ribosylation, which is crucial for genome stability and DNA repair.[3] Due to the up-regulation of some enzymes required for the biosynthesis of NAD$^+$ in cancer cells, a

Special Issue: Organometallics in Biology and Medicine

Received: July 6, 2012

   dx.doi.org/10.1021/om3006307 | *Organometallics* XXXX, XXX, XXX–XXX

decrease in the NAD^+ concentration can cause apoptosis of cancer cells while having little effect on normal cells.[4]

From an industrial perspective, NADH regeneration is an important process due to its high applicability in chiral organic synthesis and biocatalysis. The coenzymes, for instance, are required as substrates for many enzymatic reactions used for stereoselective synthesis, such as formation of D-lactate from pyruvate or chiral alcohols by alcohol dehydrogenases.[5,6]

Due to the high cost of NAD^+ and NADH, their stoichiometric use in organic synthesis, biocatalysis, or enzymatic reactions is not sustainable, hence the development of nicotinamide adenine dinucleotide models.[7] The capability of regenerating 1,4-NADH has been the subject of intense studies by enzymatic, chemical, photochemical, or electrochemical reactions.[8,9]

Recently, NADH/NAD^+ regeneration under mild conditions in aqueous media has been studied.[10,11] Significant attention has focused on transition metal complexes as catalysts for regeneration of NADH via hydrogenation[10] (H_2) or transfer hydrogenation using 2-propanol,[12] glycerol,[13] phosphate,[14] formic acid together with a base,[15] or formate[11] as the hydride source in water. Some Ru^{II},[16] Rh^{III},[17,18] and Ir^{III} [19] half-sandwich complexes can catalyze the hydrogenation or transfer hydrogenation of ketones,[20] aldehydes,[21] imines,[22] or carbon dioxide,[23] although the optimum conditions for the reactions are usually not biologically relevant. In some cases the hydride adducts can be isolated, showing that the mechanism involves hydride formation.[24,25] Of particular interest in this field are ruthenium complexes that employ Noyori's chelating ligand Ts-DPEN (*N*-[(1*R*,2*R*)-2-amino-1,2-diphenylethyl]-4-toluenesulfonamide) and its derivatives, which have achieved high enantioselectivity in transfer hydrogenation of ketones,[26] imines,[27] and C═C double bonds,[28] affording up to 97% conversions. However, the use of similar complexes under biologically relevant conditions requires high aqueous solubility and thermodynamic stability. The use of Noyori's ligand renders the complexes highly insoluble in water, due to the presence of the lipophilic phenyl groups, although recently some water-soluble complexes have been synthesized.[21,29,30] In addition, the presence of two chiral centers, which provide the complexes with enantioselectivity, makes the acquisition of a pure enantiomer a challenging process. Given that enantioselectivity is not a requirement in NAD^+/NADH catalysis, not having chiral centers offers an acceptable strategy.

We have shown previously that the Ru^{II} complexes $[(\eta^6\text{-arene})Ru(en)Cl]^+$ (arene = hmb, *p*-cym, indane (ind), and en = ethylenediamine) can reduce NAD^+ to NADH using formate as the hydride source and that such reactions might be feasible in cells because they can tolerate millimolar levels of formate.[31] However, due to the low catalytic activity of the complex, no effect was detected on A2780 human ovarian cancer cells *in vitro*. In the present work we modified the en chelating ligand by the addition of a sulfonamide group that resembles Noyori's ligand with the main goal of improving the catalytic activity of the complexes. The synthesized series of Ru^{II} complexes of the type $[(\eta^6\text{-arene})Ru(N,N')Cl]$, where N,N′ are water-soluble monosulfonate ethylenediamine ligands, *N*-(2-aminoethyl)-4-(trifluoromethyl)benzenesulfonamide (TfEn), *N*-(2-aminoethyl)-4-toluenesulfonamide (TsEn), or *N*-(2-aminoethyl)-methylenesulfonamide (MsEn), derived from Noyori's ligand Ts-DPEN (*N*-[(1*R*,2*R*)-2-amino-1,2-diphenylethyl]-4-toluenesulfonamide), were envisaged to give rise to good catalytic properties while maintaining water solubility and facilitating the synthesis and purification by avoiding enantiomeric resolution. The catalytic activity of the complexes toward the reduction of NAD^+ through transfer hydrogenation has been investigated and compared with reported ethylenediamine Ru^{II} arene complexes. The mechanism of the catalysis has also been studied both experimentally and computationally in order to compare with similar known compounds such as those reported by Steckhan and Fish.[32,33] The optimum conditions for the reaction have also been studied in relation to the potential of these complexes to act as catalytic anticancer drugs that modulate NAD^+/NADH levels in cells.

■ EXPERIMENTAL SECTION

Materials. Trihydrated ruthenium(III) trichloride was purchased from Precious Metals Online (PMO Pty Ltd.) and used as received. 4-(Trifluoromethyl)benzenesulfonyl chloride, toluenesulfonyl chloride, di-*tert*-butyl dicarbonate anhydride (*t*-BOC), hexamethylbenzene (hmb), sodium formate, β-nicotinamide adenine dinucleotide hydrate (NAD^+), and β-nicotinamide adenine dinucleotide reduced dipotassium salt (1,4-NADH) were obtained from Sigma-Aldrich. Magnesium sulfate, potassium hydroxide, sodium chloride, and hydrochloric acid were obtained from Fisher Scientific. α-Phellandrene was purchased from SAFC. Methylsulfonyl chloride, toluenesulfonyl chloride, and triflic acid were obtained from Fluka. The Ru^{II}-arene precursor dimers $[(\eta^6\text{-arene})RuCl_2]_2$ where the arene is *p*-cymene (*p*-cym), hexamethylbenzene (hmb), biphenyl (bip), or benzene (bn) were prepared following literature methods,[34] as were the ligands *N*-(2-aminoethyl)-4-(trifluoromethyl)benzenesulfonamide (TfEn)[19] and *N*-(2-aminoethyl)-4-toluenesulfonamide (TsEn).[28] The solvents used for NMR spectroscopy were purchased from Sigma-Aldrich and Cambridge Isotope Laboratories Inc. Nondried solvents used in syntheses were obtained from Fisher Scientific and Prolabo. Solvents were used as obtained, except in the case of ethanol, 2-propanol, and methanol, which were degassed prior to use by bubbling with nitrogen.

Synthesis of Ruthenium Complexes. [(*p*-cym)Ru(MsEn)Cl] (1). $[(p\text{-cym})RuCl_2]_2$ (84.2 mg, 0.138 mmol) and MsEn (101.6 mg, 0.35 mmol) were placed in a round-bottom flask to which 2-propanol (50 mL) and triethylamine (146 μL, 1.047 mmol) were added. The solution was heated under reflux in a nitrogen atmosphere overnight, after which the solvent was removed on the rotary evaporator to obtain a light brown powder. The crude product was redissolved in dichloromethane and washed with brine, after which the organic layer was dried over $MgSO_4$ and filtered. A brownish-red powder was obtained after removal of the solvent *in vacuo*. Brown crystals were obtained after recrystallization from methanol/ether (1:10 v/v) by standing in a freezer for two months at 253 K. Yield: 45.3 mg (40.4%). ^1H NMR (400 MHz, methanol-d_4): δ_H 5.59 (s, 2H), 5.42 (d, 2H, J = 5.74 Hz), 2.85 (sep, 1H, J = 7.05 Hz), 2.743 (s, 3H), 2.134 (s, 3H), 1.265 (d, 6H, J = 7.05 Hz). Anal. Calcd for $C_{13}H_{23}ClN_2O_2RuS$: C 38.28, H 5.68, N 6.87. Found C 38.27, H 5.65, N 6.82. ESI-MS: calcd for $C_{13}H_{23}ClN_2O_2RuS$ $(M - Cl)^+$ m/z 373.0, found m/z 373.0.

[(*p*-cym)Ru(TsEn)Cl] (2). Complex **2** was obtained following the method described above for complex **1** using the ligand TsEn (100.6 mg, 0.42 mmol). Recrystallization from methanol resulted in dark red crystals. Yield: 58.8 mg (36.7%). ^1H NMR (400 MHz, acetone-d_6): δ_H 7.73 (d, 2H, J = 8.25 Hz), 7.11 (d, 2H, J = 8.25 Hz), 5.85 (s, 1H), 5.71 (d, 1H, J = 5.59 Hz), 5.64 (d, 1H, J = 5.59 Hz), 5.52 (d, 1H, J = 5.59 Hz), 5.45 (d, 1H, J = 5.59 Hz), 3.24 (s, 1H), 2.94 (septet, 1H, J = 7.07 Hz), 2.84 (m,1H), 2.68 (m, 1H), 2.31 (s, 3H), 2.18 (m, 1H), 2.15 (s, 3H), 1.27 (d, 3H, J = 6.96 Hz), 1.24 (d, 3H, J = 6.96 Hz). Anal. Calcd for $C_{19}H_{27}ClN_2O_2RuS$: C 47.15, H 5.62, N 5.79. Found: C 46.70, H 5.62, N 5.79. ESI-MS: calcd for $C_{19}H_{27}ClN_2O_2RuS$ $(M - Cl)^+$ m/z 449.0, found m/z 449.0.

[(*p*-cym)Ru(TfEn)Cl] (3). Complex **3** was obtained following the method described above for complex **1** using ligand TfEn (125.0 mg, 0.47 mmol). Purification by recrystallization was not successful, and the product was used as such. Yield: 171.1 mg (85.3%). ^1H NMR (400 MHz, acetone-d_6): δ_H 8.00 (d, 2H, J = 8.12 Hz), 7.62 (d, 2H, J = 8.12

Scheme 1. Reduction of NAD^+ to 1,4-NADH in the Presence of Formate as a Hydride Source

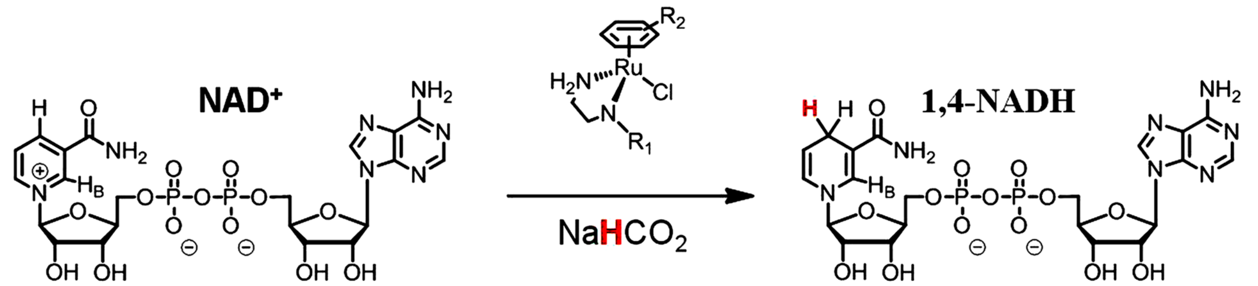

Hz), 5.74 (m, 1H), 5.51 (m, 2H), 5.41 (d, 1H), 4.23 (s, 1H), 3.27 (s, 1H), 3.10 (s, 1H), 2.76 (septet, 1H, J = 6.92), 2.75 (m, 1H), 2.29 (m, 2H), 2.17 (s, 3H), 1.27 (m, 6H). Anal. Calcd for $C_{19}H_{24}ClF_3N_2O_2RuS$: C 42.42, H 4.50, N 5.21. Found: C 41.94, H 4.45, N 5.03. ESI-MS: calcd for $C_{19}H_{24}ClF_3N_2O_2RuS$ $(M - Cl)^+$ m/z 503.0, found m/z 503.0.

[(hmb)Ru(MsEn)Cl] (4). $[(hmb)RuCl_2]_2$ (81.2 mg, 0.12 mmol) and N-(2-aminoethyl)methylsulfonamide (MsEn) (105 mg, 0.37 mmol) were dissolved in 2-propanol (25 mL). Triethylamine (155 μL, 1.11 mmol) was added, and the solution heated to reflux (363 K) under a nitrogen atmosphere for 3 h. Solvent was removed on a rotary evaporator to obtain a dark orange product. The crude product was redissolved in dichloromethane and washed with brine, after which the organic layer was dried over $MgSO_4$ and filtered. The solution was concentrated *in vacuo*, and the product recrystallized from methanol to afford an orange powder. Yield: 44.1 mg (41.6%). ^{1}H NMR (400 MHz, acetone-d_6): δ_H 2.11 (s, 18H), 2.32 (m, 2H), 2.72 (s, 3H), 2.67 (m, 2H), 4.58 (s, 2H). Anal. Calcd for $C_{15}H_{27}ClN_2O_2RuS$: C 41.32, H 6.24, N 6.43. Found: C 41.92, H 6.31, N 6.32. ESI-MS: calcd for $C_{15}H_{27}ClN_2O_2RuS$ $(M - Cl)^+$ m/z 401.0, found m/z 401.0.

[(hmb)Ru(TsEn)Cl] (5). Complex **5** was obtained following the method described above for complex **4** using ligand TsEn (64.1 mg, 0.267 mmol). The product was recrystallized from methanol, giving yellow crystals. Crystals suitable for X-ray diffraction were obtained from a methanol solution stored at 255 K. Yield: 20.5 mg (13.4%). ^{1}H NMR (400 MHz, acetone-d_6): δ_H 7.83 (d, 2H, J = 8.30 Hz), 7.07 (d, 2H, J = 8.30 Hz), 4.56 (s, 1H), 2.54 (m, 1H), 2.29 (s, 3H), 2.17 (s, 18H). Anal. Calcd for $C_{21}H_{31}ClN_2O_2RuS$: C 49.35, H 5.92, N 5.48. Found: C 49.17, H 6.04, N 5.29. ESI-MS: calcd for $C_{21}H_{31}ClN_2O_2RuS$ $(M - Cl)^+$ m/z 477.0, found m/z 477.0.

[(hmb)Ru(TfEn)Cl] (6). Complex **6** was obtained following the method described above for complex **4** using ligand TfEn (87.5 mg, 0.33 mmol). The product was recrystallized from methanol, giving red crystals. Yield: 82.2 mg (58.9%). Crystals suitable for X-ray diffraction were obtained from a methanol solution stored at 277 K. ^{1}H NMR (400 MHz, $CDCl_3$): δ_H 8.05 (d, 2H, J = 8.15 Hz), 7.56 (d, 2H, J = 8.15 Hz), 3.38 (s, 1H), 3.21 (s, 1H), 3.12 (m, 1H), 2.74 (m, 1H), 2.34 (m, 1H), 2.18 (s, 18H). Anal. Calcd for $C_{21}H_{28}ClF_3N_2O_2RuS$: C 44.56, H 4.99, N 4.95. Found: C 44.38, H 5.04, N 4.87. ESI-MS: calcd for $C_{21}H_{28}ClF_3N_2O_2RuS$ $(M - Cl)^+$ m/z 531.0, found m/z 531.0.

[(bip)Ru(MsEn)Cl] (7). $[(bip)RuCl_2]_2$ (64 mg, 0.098 mmol) and MsEn (70 mg, 0.243 mmol) were placed in a round-bottom flask and disolved in methanol (25 mL). Triethylamine (109 μL, 0.783 mmol) was added, and the solution was stirred at ambient temperature under nitrogen overnight, after which the solvent was removed on the rotary evaporator to give a dark brown product. The crude product was redissolved in dichloromethane and washed with brine, and the organic layer was dried over $MgSO_4$ and filtered. The solution was concentrated *in vacuo*, and the product recrystallized from methanol to afford red crystals. Yield: 45.2 mg (54.3%). Crystals suitable for X-ray diffraction were obtained from solution in methanol/ether (10:1 v/v) stored at 255 K. ^{1}H NMR (400 MHz, $CDCl_3$): δ_H 7.69 (m, 2H), 7.54 (m, 3H), 6.22 (t, 1H, J = 5.57 Hz), 6.01 (t, 1H, J = 5.57 Hz), 5.82 (m, 3H), 3.78 (s, 1H), 3.23 (s, 1H), 3.09 (m, 1H), 2.81 (s, 3H), 2.64 (m, 1H), 2.45 (m, 1H), 2.15 (m, 1H). Anal. Calcd for $C_{15}H_{19}ClN_2O_2RuS$: C 42.10, H 4.48, N 6.55. Found: C 41.88, H 4.49, N 6.46. ESI-MS: calcd for $C_{15}H_{19}ClN_2O_2RuS$ $(M - Cl)^+$ m/z 393.0, found m/z 393.0.

[(bip)Ru(TsEn)Cl] (8). Complex **8** was obtained following the method described above for complex **7** using ligand TsEn (69.9 mg, 0.29 mmol). The product was recrystallized from methanol to give a dark orange powder. Yield: 39.9 mg (33.9%). Crystals suitable for X-ray diffraction were obtained from a methanol solution stored at 277 K. ^{1}H NMR (400 MHz, $CDCl_3$): δ_H 2.35 (s, 3H), 2.51(m,1H), 3.08 (m, 1H), 3.22 (m, 1H), 3.68 (m, 1H), 5.77 (m, 1H), 5.96 (m, 1H), 6.03 (m, 1H), 6.39 (m, 1H), 7.17 (d, 2H, J = 7.71 Hz), 7.53 (m, 3H), 7.71 (m, 2H), 7.77 (d, 2H, J = 7.71 Hz). Anal. Calcd for $C_{21}H_{23}ClN_2O_2RuS$: C 50.04, H 4.60, N 5.56. Found: C 49.57, H 4.6, N 5.44. ESI-MS: calcd for $C_{21}H_{23}ClN_2O_2RuS$ $(M - Cl)^+$ 469.0 m/z, found 469.0 m/z.

[(bip)Ru(TfEn)Cl] (9). Complex **9** was obtained following the method described above for complex **7** using ligand TfEn (40 mg, 0.15 mmol). The product was recrystallized from methanol to give an orange solid. Yield: 45.6 mg (54.3%). ^{1}H NMR (400 MHz, $CDCl_3$): δ_H 2.17 (m, 1H), 2.31 (m, 1H), 2.55 (m, 1H), 3.11 (m, 1H), 3.21 (s, 1H), 3.74 (s, 1H), 5.80 (m, 2H), 5.95 (d, 1H, J = 5.51 Hz), 6.04 (t, 1H, J = 5.30 Hz), 6.34 (t, 1H, J = 5.82 Hz), 7.54 (m, 3H), 7.62 (d, 2H, J = 8.27 Hz), 7.70 (m, 2H), 8.00 (d, 2H, J = 8.27 Hz). Anal. Calcd for $C_{21}H_{20}ClF_3N_2O_2RuS \cdot 0.5\ H_2O$: C 44.49, H 3.52, N 4.94. Found: C 44.22, H 3.59, N 4.81. ESI-MS: calcd for $C_{21}H_{20}ClF_3N_2O_2RuS$ $(M - Cl)^+$ m/z 522.9, found m/z 522.9.0.

[(bn)Ru(MsEn)Cl] (10). $[(bn)RuCl_2]_2$ (64 mg, 0.098 mmol) and MsEn (70 mg, 0.243 mmol) were placed in a round-bottom flask and dissolved in methanol (25 mL). Triethylamine (109 μL, 0.783 mmol) was added, and the solution was stirred at ambient temperature under nitrogen overnight, after which the solvent was removed on the rotary evaporator to give a dark brown oil, which was dissolved in dichloromethane, washed with brine, dried over $MgSO_4$, and filtered. After removal of solvent on a rotary evaporator, a dark brown oil was obtained, which was washed with ether to give a brown solid. The product was recrystallized from methanol to give a brown solid. Yield: 30 mg (49.2%). ^{1}H NMR (400 MHz, $CDCl_3$): δ_H 5.67 (s, 6H), 2.80 (s, 3H). Anal. Calcd for $C_9H_{15}ClN_2O_2RuS$: C 30.73, H 4.30, N 7.96. Found: C 30.29, H 4.14, N 7.76. ESI-MS: calcd for $C_9H_{15}ClN_2O_2RuS$ $(M - Cl)^+$ m/z 317.0, found m/z 317.0.

[(bn)Ru(TsEn)Cl] (11). Complex **11** was obtained following the method described above for complex **10** using ligand TsEn (100 mg, 0.417 mmol). The crude product was recrystallized from methanol to give an orange powder. Yield: 47 mg (52.4%). ^{1}H NMR (400 MHz, $CDCl_3$): δ_H 7.75 (d, 2H, J = 7.79 Hz), 7.28 (d, 2H, J = 7.79 Hz), 5.71 (s, 6H), 4.89 (s, 1H), 3.14 (s, 1H), 3.05 (s, 1H), 2.75 (s, 1H), 2.35 (m, 1H), 2.35 (s, 3H). Anal. Calcd for $C_{15}H_{19}ClN_2O_2RuS$: C 42.10, H 4.48, N 6.55. Found: C 41.83, H 4.48, N 6.74. ESI-MS: calcd for $C_{15}H_{19}ClN_2O_2RuS$ $(M - Cl)^+$ m/z 393.0, found m/z 393.0.

[(bn)Ru(TfEn)Cl] (12). Complex **12** was obtained following the method described above for complex **10** using ligand TfEn (100 mg, 0.38 mmol). The crude product was recrystallized from methanol to give a reddish powder. Yield: 53.6 mg (59.0%). ^{1}H NMR (400 MHz, $CDCl_3$): δ_H 7.99 (d, 2H, J = 8.2 Hz), 7.62 (d, 2H, J = 8.2 Hz), 5.73 (s, 6H), 4.71 (s, 1H), 3.12 (m, 2H), 2.79 (m,1H), 2.25 (m, 2H). Anal. Calcd for $C_{15}H_{16}ClF_3N_2O_2RuS$: C 37.39, H 3.35, N 5.81. Found: C

dx.doi.org/10.1021/om3006307 | *Organometallics* XXXX, XXX, XXX−XXX

37.00, H 3.39, N 5.81. ESI-MS: calcd for $C_{15}H_{16}ClF_3N_2O_2RuS$ $(M - Cl)^+$ *m/z* 446.9, found *m/z* 446.9.

NAD^+ Reduction. Complexes **1**−**12** were dissolved in D_2O or $MeOD/D_2O$ (5:1 v/v) (1.4 mM, 4 mL) in a glass vial. Solutions of sodium formate (35 mM, 4 mL) and NAD^+ in D_2O (2.8 mM, 2 mL) were also prepared and then incubated at 310 K. In a typical experiment an aliquot of 200 μL from each solution was added to a 5 mm NMR tube, and the pH* adjusted to 7.2 ± 0.1, bringing the total volume to 0.635 mL (final concentrations were Ru complex 0.44 mM; NAD^+ 0.88 mM; $NaHCO_2$ 11.02 mM; molar ratio 1:2:25). A ^1H NMR spectrum was recorded at 310 K every 162 s until the completion of the reaction.

Molar ratios of NAD^+ and NADH were determined by integrating the peaks corresponding to H_B (Scheme 1) of NAD^+ (9.33 ppm) and H_B of 1,4-NADH (6.96 ppm). The turnover number (TON) for the reaction was calculated as follows:

$$\mathrm{TON} = \frac{I_{6.96}}{I_{6.96} + I_{9.93}} \frac{[\mathrm{NAD}^+]_0}{[\mathrm{Catalyst}]}$$

where I_n is the integral of the signal at n ppm and $[NAD^+]_0$ is the concentration of NAD^+ at the start of the reaction.

A series of experiments were performed where complex **2** (2.71 mg, 0.0056 mmol) was dissolved in D_2O (1.4 mM, 4 mL) in a vial. Following the same procedure used above, the kinetics of the reaction was studied using different concentrations of NAD^+ (1, 2, 3, 4, and 6 molar equiv). A second series of experiments using different concentrations of sodium formate (2, 5, 10, 25, 50, 100, and 200 molar equiv) were also performed. ^1H NMR spectra were recorded at 310 K every 162 s until completion of the reaction in both cases.

The optimum pH range for the catalytic reaction was studied by a series of kinetic experiments following the same procedure described above. In each experiment the pH* was adjusted to 6, 6.5, 7, 7.2, 7.5, 8, and 10. The effect of added methanol on the reaction rate was studied by six experiments containing different quantities of methanol (0, 5, 10, 23.3, 50, 66.6% v/v of d_4-MeOD in D_2O).

NMR Spectroscopy. ^1H NMR spectra were acquired in 5 mm NMR tubes at 298 or 310 K on either a Bruker DPX-300, AV-400, DRX-500, or AV III 600 spectrometer. Data processing was carried out using XWIN-NMR version 3.6 (Bruker U.K. Ltd.). ^1H NMR chemical shifts were internally referenced to TMS via 1,4-dioxane in D_2O (δ = 3.75) or residual DMSO (δ = 2.52 ppm), acetone (δ = 2.05 ppm), MeOH (δ = 3.31 ppm), or $CHCl_3$ (δ = 7.26 ppm). 1D spectra were recorded using standard pulse sequences. Typically, data were acquired with 16 transients into 32 k data points over a spectral width of 14 ppm and, for the kinetic experiment, 32 transients into 32 k data points over a spectral width of 30 ppm using a relaxation delay of 2 s.

pH* Measurements. pH values were measured at ambient temperature using a Minilab IQ125 pH meter equipped with a ISFET silicon chip pH sensor and referenced in KCl gel. The electrode was calibrated with Aldrich buffer solutions of pH 4, 7, and 10. pH* values (pH meter reading without correction for the effect of deuterium on a glass electrode) of NMR samples in D_2O were measured at 310 K. pH* values were adjusted with KOH or $HClO_4$ solutions in D_2O.

Elemental Analysis. Elemental analyses were performed by Warwick Analytical Service using an Exeter Analytical elemental analyzer (CE440).

Electrospray Ionization Mass Spectrometry (ESI-MS). Positive ion electrospray mass spectra were obtained on a Bruker Daltonics Esquire 2000 ion trap mass spectrometer. All samples were prepared in water/acetonitrile (20:80 v/v) or methanol (100%). Data were processed using Data-Analysis version 3.3 (Bruker Daltonics).

X-ray Crystallography. Diffraction data were collected on an Oxford Diffraction Gemini four-circle system with a Ruby CCD area detector. All structures were refined by full-matrix least-squares against F^2 using SHELXL 97[35] and were solved by direct methods using SHELXS[36] (TREF) with additional light atoms found by Fourier methods. Hydrogen atoms were added at calculated positions and refined using a riding model, except the hydrogens on the NH nitrogens, which were located in a difference map. Anisotropic displacement parameters were used for all non-H atoms; H atoms were given an isotropic displacement parameter equal to 1.2 (or 1.5 for methyl and NH H atoms) times the equivalent isotropic displacement parameter of the atom to which they are attached. The data were processed by the modeling program Mercury 1.4.1.

X-ray crystallographic data for complexes **1**, **5**, **6**, **7**, and **8** are available as Supporting Information and have been deposited in the Cambridge Crystallographic Data Centre (CCDC reference numbers 885977, 885979, 885978, 885976, and 885980, respectively).

Computational Details. All calculations used the ORCA program version 2.8.[37] Minimum-energy structures and transition states were located using the OPBE functional, spin restricted, in conjunction with the def2-TZVP basis sets and the resolution of identity approximation.[38,39] Solvation effects were included via the conductor-like screening model implemented in ORCA with water as the solvent. Stationary points were confirmed as local minima or transition states via numerical frequency calculations. Final free energies were computed using the statistical mechanics corrections computed from the OPBE optimizations with B3LYP energies using the def2-TZVP basis sets plus the COSMO solvation corrections[40] and Grimme's empirical correction for dispersion.[41]

■ RESULTS

Synthesis and Characterization. Ru^{II} complexes **1**−**12** were synthesized (Chart 1) using a similar procedure. Typically, triethylamine (4−6 molar equiv) and the ligand (2−2.5 molar equiv) were added to an alcoholic solution of the ruthenium dimer $[(\eta^6\text{-arene})RuCl_2]_2$, and the reaction mixture was stirred under a N_2 atmosphere under reflux or at ambient temperature. The details for individual reactions are described in the Experimental Section. All the synthesized complexes were characterized by elemental analysis (CHN), mass spectrometry (ESI-MS), and ^1H NMR spectroscopy. X-ray crystal structures for complexes **1** and **5**−**8** were obtained. ^1H NMR spectra were fully assigned although peaks corresponding to the CH_2 of the chelating ethylenediamine backbone, expected between 2 to 4 ppm, were broad.

Chart 1. Ruthenium Arene Complexes Studied in This Work

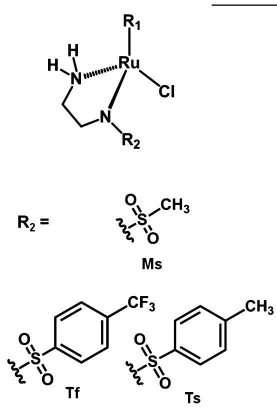

Complex	R₁ (Arene)	R₂
1	*p*-cym	Ms
2	*p*-cym	Ts
3	*p*-cym	Tf
4	hmb	Ms
5	hmb	Ts
6	hmb	Tf
7	bip	Ms
8	bip	Ts
9	bip	Tf
10	bn	Ms
11	bn	Ts
12	bn	Tf

X-ray Crystal Structures. Crystallographic data for complexes **1** and **5**−**8** are listed in Table S1, and selected bond lengths and angles in Tables 1 and 2. Their molecular structures are depicted in Figure 1. These complexes adopt the familiar pseudo-octahedral "piano-stool" geometry with the η^6-bonded arene occupying one face of the complex. Complexes **1**, **5**, **7**, and **8** were obtained in an enantiomerically pure form. The chelating ligand appeared to be deprotonated and

Table 1. Selected Bond Lengths (Å) and Angles (deg) for Complexes 1, 5, 7, and 8

	5[a]	8[a]	1[b]	7[b]
Ru1−Na	2.141(3)	2.122(3)	2.1331(15)	2.1276(19)
Ru1−N⁻	2.129(3)	2.096(4)	2.1339(13)	2.1073(16)
Ru1−Cl1	2.4146(8)	2.4444(11)	2.4425(4)	2.4331(6)
Ru1−arene (centroid)	1.6742	1.6742	1.672	1.672
N⁻−Ru1−Na	78.00(11)	78.54(14)	78.74(6)	77.80(7)
Na−Ru1−Cl1	89.44(8)	85.44(11)	87.91(4)	82.57(6)
N⁻−Ru1−Cl1	85.63(8)	82.97(11)	84.53(5)	88.61(5)

[a]N⁻ corresponds to N4; Na corresponds to N1. [b]N⁻ corresponds to N3; Na corresponds to N6.

Table 2. Selected Bond Lengths (Å) and Angles (deg) for the Three Crystallographically Independent Molecules of Complex 6

	6a[a]	6a′[b]	6b[c]
Ru1−N⁻	2.116(2)	2.1234(18)	2.133(2)
Ru1−Na	2.151(2)	2.134(2)	2.142(2)
Ru1−Cl1	2.4344(6)	2.4229(6)	2.4240(6)
Ru1−arene$_{centroid}$	1.679	1.675	1.674
N⁻−Ru1−Na	77.58(8)	77.69(8)	77.54(8)
Na−Ru1−Cl1	90.39(6)	87.49(5)	89.43(5)
N⁻−Ru1−Cl1	84.74(6)	84.81(6)	84.64(6)

[a]N⁻ corresponds to N104; Na corresponds to N101. [b]N⁻ corresponds to N204; Na corresponds to N201. [c]N⁻ corresponds to N304; Na corresponds to N301.

coordinated as a monoanionic bidentate *N,N′*-ligand (amine and amide coordination). A chloride anion completes the coordination sphere around ruthenium. Especially interesting for further discussion are the distances Ru−Cl 2.4444(11) Å for [(bip)Ru(TsEn)Cl] (**8**), 2.4331(6) Å for [(bip)Ru(MsEn)Cl] (**7**), 2.4425(4) Å for [(*p*-cym)Ru(MsEn)Cl] (**1**), 2.4146(8) Å for [(hmb)Ru(TsEn)Cl] (**5**), and 2.4344(6), 2.4229(6), and 2.4240(6) Å for [(hmb)Ru(TfEn)Cl] (**6**).

X-ray diffraction studies for complex **6** showed three crystallographically independent structures in the asymmetric unit (Figure S1): **6a** and **6a′** correspond to one enantiomer; **6a′** forms an H-bond to MeOH and **6b** to the other enantiomer.

Hydrolysis and pK_a of Aqua Complexes. Hydrolysis of complex **2** was studied since the formation of an aqua complex is a possible first step in the catalytic cycle. When the complex was dissolved in D_2O (1.4 mM), no changes were observed by ^{1}H NMR after 24 h. The peaks in the ^{1}H NMR spectra can be assigned to the aqua complex since the chemical shifts of the resonances correlate to those obtained for the aqua complex (prepared by the addition of silver nitrate (1 molar equiv) in water). The rate of aquation was too fast to be determined by ^{1}H NMR.

The changes in the ^{1}H NMR chemical shifts of the *p*-cymene protons in the aqua adduct of complex **2** (1.4 mM) were followed by changing the pH* ranging from 2 to 12. The data were fitted to the Henderson−Hasselbalch equation, which resulted in a pK_a* of 9.06 (Figure S2).

Kinetics of Transfer Hydrogenation Reactions. Catalytic transfer hydrogenation of nicotinamide adenine dinucleotide (NAD^+) in aqueous media using complexes **1**−**12** as catalyst and formate as a hydride source (25 molar equiv) was studied by ^{1}H NMR at 310 K and pH* 7.2 ± 0.1. Spectra were recorded every 162 s until completion of the reaction. In order to compare the catalytic activity of the complexes and due to the poor solubility of complexes **6**−**9**, the experiments were also performed in the mixed solvent MeOD/D_2O (2:9 v/v).

The reaction was regioselective, giving 1,4-NADH in 93% yield when complex [(hmb)Ru(MsEn)Cl] (**4**) was used, and a similar regioselectivity was achieved with complexes containing hexamethylbenzene (**5** and **6**). When using *p*-cymene complexes **1**, **2**, and **3**, the 1,6-NADH adduct was also produced (up to 16%), with complex [(*p*-cym)Ru(TfEn)Cl] (**3**) giving the lowest regioselectivity from the three *p*-cymene

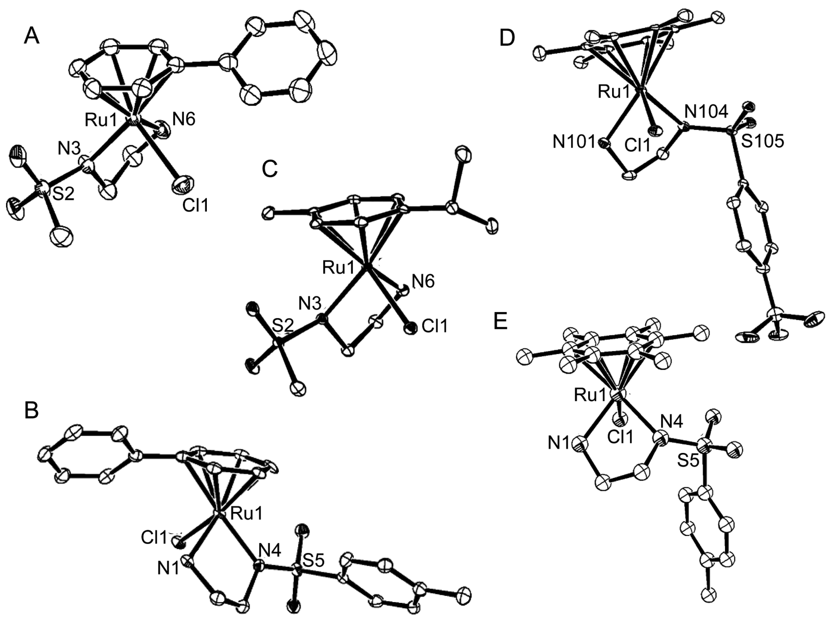

Figure 1. ORTEP diagrams for complexes (A) **7**, (B) **8**, (C) **1**, (D) **6**, and (E) **5**. Ellipsoids are shown at the 50% probability level. All hydrogen atoms and solvent molecules have been omitted for clarity.

complexes. Finally complexes **10**, **11**, and **12**, containing benzene as arene, gave 23–25% of 1,6-NADH.

Molar ratios of NAD^+ and NADH (Scheme 1) were determined by integrating the signals corresponding to H_B of NAD^+ (9.33 ppm) and H_B of 1,4-NADH (6.96 ppm; Scheme 1). The turnover numbers for the reactions were determined as described in the Experimental Section. An important effect of adding methanol to the reaction mixture on the TON was discovered (*vide infra*). The turnover frequencies (TOF, the increment of turnover number over time), Table 3, showed a marked dependence of the catalytic activity on the arene. Complexes of the type [(arene)Ru(XEn)Cl], where X is Tf, Ts, or Ms, are more active when the arene is benzene, and activity decreases in the order bn > bip > *p*-cym > hmb. It was also evident from the turnover frequencies that catalytic activity depends on the N,N′-ligand. The complex with the electron-withdrawing chelated ligand sulfonamide substituent (TfEn) exhibited the highest activity, while the complex with the least electron-withdrawing sulfonamide substituent (MsEn) was the least active (Table 3). [(bn)Ru(TfEn)Cl] (**12**), with a TOF of 10.4 h^{-1}, was the most active.

Table 3. Turnover Frequencies for Transfer Hydrogenation Reactions Using Catalysts 1–12

complex	R_1 (arene)	R_2	TOF (h^{-1}) D_2O/MeOD[a]	TOF (h^{-1}) D_2O
1	*p*-cym	Ms	1.25	1.11
2	*p*-cym	Ts	2.88	1.58
3	*p*-cym	Tf	5.77	3.06
4	hmb	Ms	0.15	0.14
5	hmb	Ts	0.38	0.34
6	hmb	Tf	1.47	—[b]
7	bip	Ms	3.04	—[b]
8	bip	Ts	4.28	—[b]
9	bip	Tf	7.45	—[b]
10	bn	Ms	4.09	2.94
11	bn	Ts	6.76	4.50
12	bn	Tf	10.39	6.62

[a]23% v/v MeOD/D_2O. [b]Not soluble in D_2O.

Mechanistic Studies. The rate-limiting step of the catalytic cycle for NAD^+ reduction was investigated by studying the reaction of complex **3** with deutero-formate (25 molar equiv) as a deuteride source. The turnover frequency (1.96 h^{-1}) was 2.4 times smaller than that obtained using formate as the hydride source.

The dependence of the rate of catalytic activity on concentration of NAD^+ and formate was also determined using complex **2** as a model system. Accordingly five experiments were performed with complex **2**, sodium formate, and NAD^+ in the ratio of 1:25:X, respectively, where X = 1, 2, 3, 4, or 6 molar equiv, and the ^1H NMR spectra were recorded every 2 min until 100% conversion was achieved. The analysis of the experiments gave an unchanged turnover frequency (2.88 h^{-1}).

A second series of experiments were performed in order to investigate the dependence of the reaction rate on the formate concentration. Experiments with complex **2**, sodium formate, and NAD^+ in the ratio 1:X:2, respectively, where X = 2, 5, 10, 25, 50, 100, or 200 molar equiv of formate, were performed. The plot of the data obtained shows a strong dependence of the turnover frequency on formate concentration (Figure 2). Typical Michaelis–Menten kinetic behavior is apparent from a plot of turnover frequency versus formate concentration. Thus, from the double-reciprocal plot (Figure 3) the Michaelis constant (K_M = 27.8 mM) and the maximum turnover frequency (TOF_{max} = 6.4 h^{-1}) were calculated.

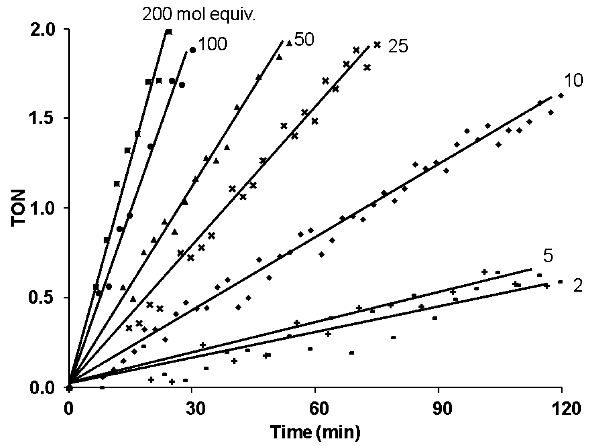

Figure 2. Dependence of the turnover number on time for the reduction of NAD^+ by complex **2** using formate as a hydride source (mol ratio 2:1:X, X = 2, 5, 10, 25, 50, 100, or 200. pH* 7.4, 310 K, D_2O).

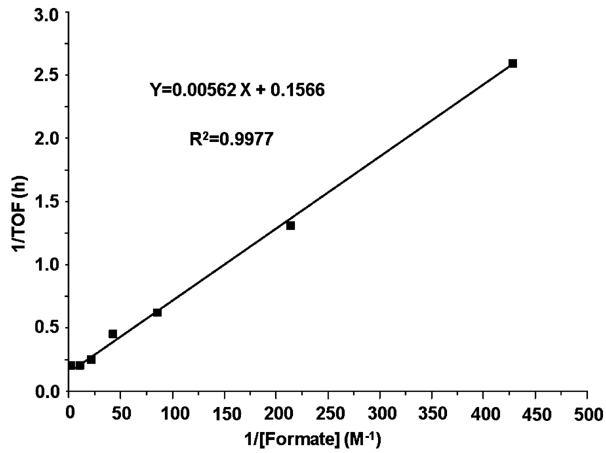

Figure 3. Plot of the reciprocal of the TOF against formate concentration for the reduction of NAD^+ in the presence of various molar equiv of formate, catalyzed by complex **2**. For a reaction following Michaelis-type kinetics, TOF = $TOF_{max}[S]/(K_m + [S])$, where TOF_{max} is the turnover frequency at infinite substrate (formate) concentration, [S] is the substrate concentration, and K_m is the Michaelis constant. Hence, $TOF^{-1} = (K_m/TOF_{max})(1/[S]) + (1/TOF_{max})$, and K_m and TOF_{max} can be obtained from the gradient and y intercept, respectively, of the double-reciprocal plot.

The pH* dependence of the catalytic reaction ranging from 6 to 10 was also investigated via a series of experiments using complex **2**, sodium formate, and NAD^+ (ratio 1:25:2, respectively) in D_2O. A strong dependence on pH* was found. The highest TOF (1.58 h^{-1}) was achieved at pH* 7.2, followed by a decrease in the activity when the pH* increased (Figure S3).

The catalytic activity of all the complexes was initially studied in D_2O, but complexes **6**–**9** could not be dissolved to the same concentration (1.4 mM). For this reason experiments were also performed in a D_2O/methanol (9:2 v/v) mixture in order to increase the solubility. The addition of methanol in the reaction mixture resulted in higher turnover frequencies (Table 3) for catalysts **1**−**5** and **10**−**12** compared to in D_2O alone. In order to study the effect of methanol in the reaction, five experiments with catalyst **2**, sodium formate, and NAD^+ (ratio 1:25:2, pH* 7.2, 310 K) were performed in D_2O/MeOD (5, 10, 23.3, 50, or 66.6% v/v). The higher percentage of methanol resulted in an increase in the rate of the reaction and therefore higher turnover frequency (Figure S4).

DFT Calculations. A DFT mechanistic study was performed initially with the aqua complex $[(bn)Ru(MsEn)(H_2O)]^+$ (**10**) in the presence of formate. The energy of the formate complex plus water was found to be lower than the energy of the aqua complex plus formate, so the formate complex was taken as the reference point for determining barriers to CO_2 elimination.

Formate coordinates via a single oxygen with the carbonyl moiety making an H-bond with an NH proton (Figure 4). It

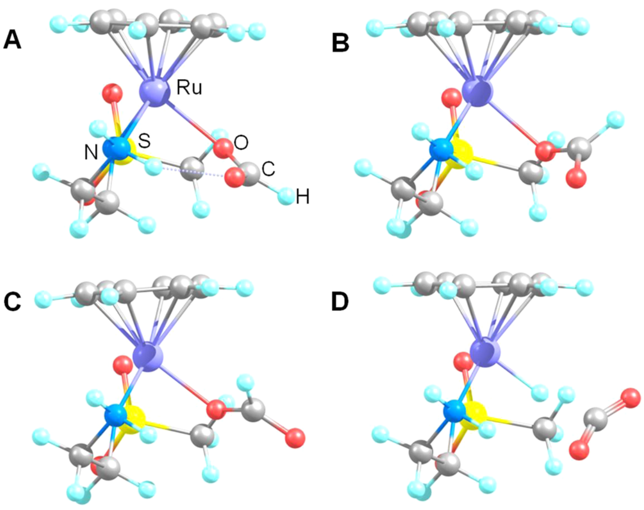

Figure 4. Calculated DFT structures for the formate adduct of $\{(bn)Ru(MsEn)\}^+$ (from **10**). (A) Intermediate complex with formate bound via a single oxygen with an H-bond between the second formate oxygen and NH from the chelating ligand. (B) Transition state for the rotation of formate that begins to orient the hydrogen toward the metal center. (C) Intermediate showing the hydrogen now oriented toward the Ru center, and finally (D) the transition state for the formation of the ruthenium−hydride bond and CO_2 elimination. Imaginary frequencies for B and D were 148i and 329i cm^{-1}, respectively.

then rotates via a low-energy transition state to an intermediate with the formate H now oriented toward the Ru center. From here, the Ru−H bond is formed via a higher energy transition state (TS). The energetics of this process and for CO_2 elimination for the formate adducts of the bn complexes $\{(bn)Ru(MsEn)\}^+$ (**10**), $\{(bn)Ru(TsEn)\}^+$ (**11**), and $\{(bn)Ru(TfEn)\}^+$ (**12**) and for the formate adduct of the hmb complex $\{(hmb)Ru(MsEn)\}^+$ (**4**) are collected in Table 4.

DISCUSSION

Structures of the Complexes. The ligands TsEn, TfEn, and MsEn were selected in order to compare the catalytic properties of complexes of the type [(arene)Ru(XEn)Cl], where X is Ms, Ts, or Tf, with an increasing electron-withdrawing power of the sulfonamide. Enantiomerically pure single crystals of complexes [(*p*-cym)Ru(MsEn)Cl] (**1**), [(hmb)Ru(TsEn)Cl] (**5**), [(bip)Ru(MsEn)Cl] (**7**), and [(bip)Ru(TsEn)Cl] (**8**) were obtained and analyzed by X-ray diffraction. The crystal structure of complex [(hmb)Ru(TfEn)Cl] (**6**) shows an asymmetric unit containing three crystallographically independent molecules. One of the ruthenium molecules (**6a**) establishes an intermolecular hydrogen bond with a methanol molecule (Table S4). The other two molecules (**6a′** and **6b**) are enantiomers with similar bond lengths and angles (Table 3), which are slightly different from those of complex **6a**.

Table 4. Computed DFT(B3LYP) Free Energy Barriers $\Delta G^\ddagger$ (kcal mol^{-1}) Leading to CO_2 Elimination

complex	$\Delta G^\ddagger$ twist	$\Delta G^\ddagger$ CO_2 elim
10	5.9	13.7
11	4.2	12.9
12	4.2	12.6
4		18.1

Comparison with the analogous ethylenediamine complex[42,43] shows no significant difference between the Ru−NH_2 bond length and that of Ru−N^- despite the higher electron density on the imino nitrogen: 2.130(3) Å for $[(p\text{-cym})Ru(en)Cl]^+$, 2.1331(15) Å for [(*p*-cym)Ru(MsEn)Cl] (**1**), 2.109(3) Å for $[(bip)Ru(en)Cl]^+$, and 2.096(4) and 2.1073(16) Å for complexes **8** and **7**, respectively. However, comparing the complexes containing hmb, the Ru−N^- bond length is slightly shorter (ca. 0.02−0.03 Å). The respective Ru−Cl bond lengths in complexes **1**, **5**, **6**, **7**, and **8** (2.4146(8)−2.4444(11) Å) are within the range displayed by other compounds of the type $[(\eta^6\text{-arene})Ru(en)Cl]^+$ (2.41−2.44 Å).[42]

When the Ru−N^- and the Ru−Cl bond lengths of the complexes with different η^6-arene but the same N,N′ chelating ligand (**1**, **7**, **5**, and **8**) are compared, each differs by ca. 0.03 and 0.01−0.03 Å, respectively. Similarly, comparing the influence of the chelating ligand when the same arene is used, an increase in the electron-withdrawing power of the R_2 group (Tf > Ts > Ms) appears to increase the Ru−Cl bond length, whereas the Ru−N^- bond length decreases.

Hydrolysis and Acidity of the Aqua Complex. Aquation of the complexes in D_2O was confirmed by comparison of the ^1H NMR spectra of the solution of complex **2** in D_2O and the solution obtained after removal of the chloride by reaction with silver ions ($AgNO_3$). Hydrolysis of **2** appeared to be rapid under biologically relevant conditions (310 K, pH* 7.2), since equilibrium was reached by the time the first ^1H NMR spectrum was recorded (<6 min). Consequently the turnover frequency for the transfer hydrogenation to form NAD^+ does not depend on whether the chlorido or aqua adduct is used.

A ^1H NMR pH* titration of **2** gave a pK_a* value of 9.06 for the aqua ligand (Figure S3). These results suggest that complex **2** would exist mainly as the aqua adduct over the pH* range used during the experiment, which was close to physiological pH (7.4).

Mechanism of the Catalytic Reduction of NAD^+. Use of deuterated formate and complex **3** gave a turnover frequency 2.4 times smaller than that with formate. Since the rate of formation of the hydride (*β*-elimination) with the heavier atom is lower, the difference in the turnover frequency between the two reactions suggests that the rate-limiting step of the reaction is the formation of Ru−H. To determine the factors that influence the reaction rate, a series of experiments with complex **2** were performed by varying the concentration of the different

Scheme 2. Proposed Mechanism for Reduction of NAD^+ to 1,4-NADH via Transfer Hydrogenation Using Formate as the Hydride Source[a]

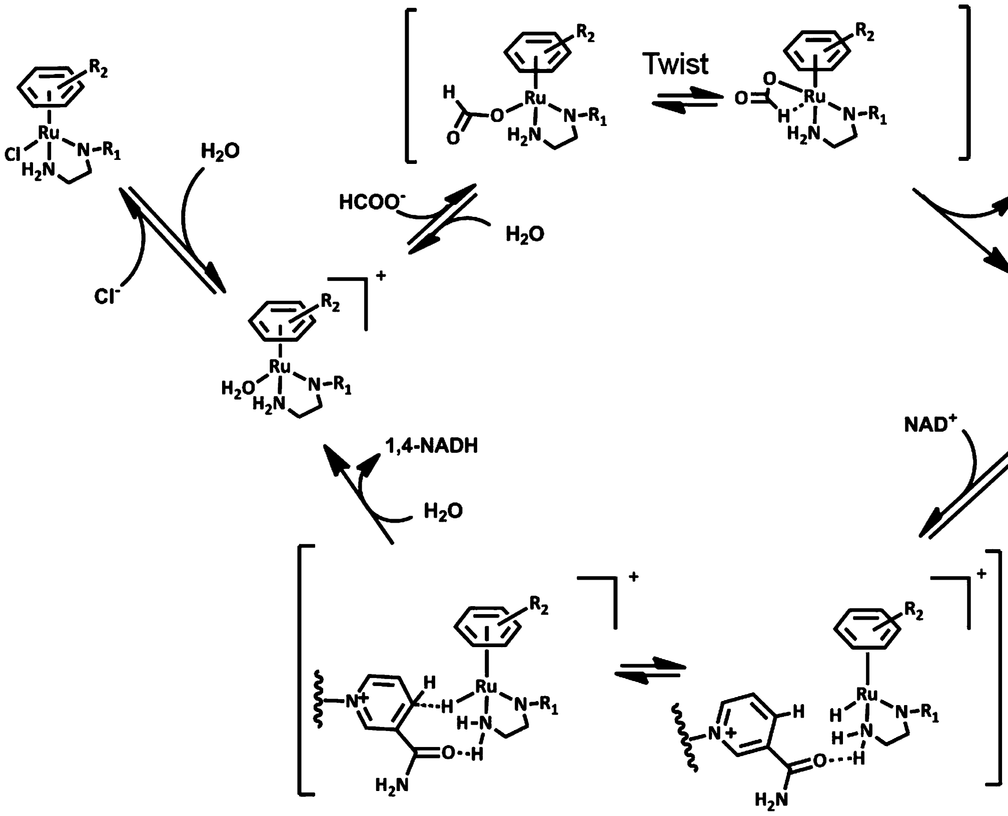

[a] R_1 = Ms (SO_2CH_3), Ts ($SO_2(C_6H_4)CH_3$), or Tf ($SO_2(C_6H_4)CF_3$); Arene-R_2 is *p*-cym, hmb, bip, or bn.

reactants. When the NAD^+ concentration was changed, no significant alterations in the rate were observed, implying that the reaction rate does not depend on the NAD^+ concentration. However the reaction rate decreased with lower concentrations of the hydride source (sodium formate), suggesting that formate is involved in the rate-determining step (Figure 2).

The plot of turnover frequency against formate concentration showed Michaelis–Menten behavior (Figure 3). The maximum turnover frequency for complex **2** (TOF_{max} = 6.4 h^{-1}) is about 4 times higher than that previously determined for the en complex [(hmb)Ru(en)Cl]$^+$ (TOF_{max} = 1.46 h^{-1}),[31] so achieving the desired increased efficiency in the reaction.

On the basis of the data obtained, we can propose a plausible catalytic cycle for the reduction of NAD^+ via transfer hydrogenation with formate as a hydride source (Scheme 2). This cycle is comparable with that established by Fish et al.[33] for the reduction of NAD^+ via transfer hydrogenation using [(Cp*)Rh(bipy)H_2O]$^{2+}$ as the catalyst and formate as hydride source. In the first step, the precatalyst chlorido complex is converted to the aqua adduct. The reaction of the aqua complex with $HCOO^-$ generates the formate adduct [(arene)-Ru(N,N′)(OHCO)]. The formate coordinates via a single oxygen with the carbonyl moiety making an H-bond with an NH proton. It then rotates to form an intermediate with the formate H now oriented toward the Ru center. From here, the formate adduct undergoes decomposition to the hydride complex [(arene)Ru(N,N′)(H)], through a *β*-elimination reaction and generation of CO_2.[33] Transfer of hydride to produce 1,4-NADH regenerates the aqua adduct.

The low Michaelis constant (K_m = 27.8 mM) indicates a stronger affinity of the complex for formate compared to the complexes [(hmb)Ru(en)Cl]$^+$ (K_m = 58 mM)[31] and [(Cp*)-Rh(bipy)H_2O]$^{2+}$ (K_m = 140 mM),[33] while the maximum turnover frequency (TOF_{max} = 6.4 h^{-1}) of the reaction indicated an increase in the catalytic activity compared to [(hmb)Ru(en)Cl]$^+$ (TOF_{max} = 1.46 h^{-1}),[31] but lower catalytic activity compared with the complex [(Cp*)Rh(bipy)H_2O]$^{2+}$ (TOF = 77.5 h^{-1}).[33] Several other Ru, Rh, and Ir complexes have previously been reported to catalyze the regioselective reduction of NAD^+ to 1,4-NADH using formate as a hydride source.[44,45] The complexes studied in the present work show comparable TOFs (ca. 0.2–7 h^{-1}) to reported [(η^6-arene)Ru-(NN′)Cl] complexes (ca. 0.0056–10 h^{-1}), although the TOFs displayed are much lower than those for some Rh or Ir complexes.[44,45] The maximum activity for complex **2** was observed at pH* 7.2 (Figure S3). At higher pH* the concentration of OH^- inhibits the reaction, and at pH* 10 or higher the complex decomposes. The experiments with complexes **1**–**12** as catalysts were performed in D_2O and in a mixture of D_2O/methanol (9:2 v/v). The addition of methanol resulted in an increase in the turnover frequency compared to in D_2O alone.

The DFT energetics correlate well with other experimental data and predict increasing barriers (and hence slower reactions) for bn complexes in the order TfEn (**12**) < TsEn (**11**) < MsEn (**10**), although it should be noted that the difference between barriers is small (ca. 1.1 kcal mol^{-1}). For MsEn, the barrier for {(hmb)Ru(MsEn)}$^+$ (**4**) is substantially larger than for {(bn)Ru(MsEn)}$^+$ (**10**), which also agrees with experiment. Overall, the computational protocol appears to provide a very good description of these systems. DFT thus could provide, in the future, a useful tool to help the *a priori* design of new complexes with desired properties.

Kinetics of Transfer Hydrogenation Reactions. The catalytic reduction of NAD^+ under biologically relevant conditions (310 K, pH* 7.2) using complexes **1**−**12** as catalysts and formate as a hydride source showed a general tendency in which the more electron-withdrawing sulfonamides on the chelating ligand achieved higher catalytic activity. Accordingly, complexes using TfEn as chelating ligand are more active than those with the TsEn ligand, and, in turn, both are more active than the complexes containing the MsEn ligand. Such a trend has been previously reported in the catalytic transfer hydrogenation of aldehydes[46] and quinoxalines.[19]

The nature of the arene had a dramatic effect on the reaction rate. Electron-poor arene ligands such as benzene are reported to accept electron density from the central Ru^{II}. Consequently the lower electron density on the Ru^{II} center for complexes [(bn)Ru(N,N′)Cl] (**10**, **11**, and **12**) compared to complexes [(hmb)Ru(N,N′)Cl] (**4**, **5**, and **6**) stabilizes the coordination of the negatively charged formate to Ru, making the hydride transfer from formate more difficult.[47,48] However, the experimental data show higher catalytic activity when the arene is more electron deficient (Table 3), [(bn)Ru(N,N′))Cl] being the more active complexes while [(hmb)Ru(N,N′)Cl] are less active. This unexpected trend may be due to steric hindrance since the more sterically hindered arene (hmb) shows lower activity while the less sterically hindered arene (bn) shows higher activity.

■ CONCLUSIONS

In this work we have studied a series of water-soluble Ru^{II} half-sandwich complexes of the type [(η^6-arene)Ru(N,N′)(Cl)] where N,N′ are monosulfonamide chelating ligands derived from ethylenediamine. The X-ray crystal structures of complexes **1** and **5**−**8** showed the familiar piano stool geometry common to all [(η^6-arene)Ru(X,Y)(L)] compounds. Particularly interesting is the effect of the more electron-withdrawing sulfonamide groups from the chelating ligand on weakening the Ru−Cl bond. Longer Ru−Cl distances appear to correlate with an increase in catalytic activity. The ability of the complexes to act as catalysts for the regioselective transfer hydrogenation of NAD^+ to form 1,4-NADH was studied. The catalytic activity decreases in the order TfEn > TsEn > MsEn, showing that more electron-withdrawing sulfonamides increase the activity. The nature of the arene significantly influences the catalytic activity. Benzene complexes are the most active, while the activity decreases in the order biphenyl > *p*-cymene > hexamethylbenzene. Complex [(bn)Ru(TfEn)Cl] (**12**) was the most active, with a TOF of 10.4 h^{-1}. Mechanistic studies on complex **2** [(*p*-cym)Ru(TsEn)(Cl)] showed a dependence of the reaction rate on formate, but not on NAD^+ concentration. The formation of the hydride complex was shown to be the rate-limiting step through deuterium isotope experiments. DFT calculations were performed for the coordination of formate and subsequent CO_2 elimination to generate the hydride complex. The elimination of CO_2 occurs via a two-step process with the coordinated formate first twisting to present its hydrogen toward the metal center followed by β-elimination and Ru−H formation. The computed barriers for complexes using η^6-benzene follow the order MsEn > TsEn > TfEn, and for the MsEn chelating system the barrier follows the order bn < hmb, both consistent with the observed rates. Finally optimum pH* was found to be 7.2, which is close to physiological pH. The series of compounds studied here showed improved catalytic activity that is an order of magnitude higher than that of the ethylenediamine analogues, which could be significant if such catalytic reactions are to be used to modulate NADH levels in cells.

■ ASSOCIATED CONTENT

Supporting Information

Ligand synthesis, titration of complex **2** (Figure S2), pH-dependent study of the reaction (Figure S3), methanol effect (Figure S4), and crystallographic data (Figure S1, Tables S1−S6). This material is available free of charge via the Internet at http://pubs.acs.org. X-ray crystallographic data in CIF format are available from the Cambridge Crystallographic Data Centre (http://www.ccdc.cam.ac.uk).

■ AUTHOR INFORMATION

Corresponding Author

*E-mail: p.j.sadler@warwick.ac.uk.

Author Contributions

§These authors contributed equally.

Funding

We thank ERDF/AWM (Science City), NWO (Rubicon grant), EPSRC (grant no. EP/F042159/1), and ERC (grant no. 247450) for support of this work, and J.A.S.C. for a scholarship for J.J.S.B.

Notes

The authors declare no competing financial interest.

■ ACKNOWLEDGMENTS

We thank Dr. Ivan Prokes, Dr. Lijiang Song, and Mr. Philip Aston (University of Warwick) for their excellent assistance with the NMR and MS instruments.

■ REFERENCES

(1) Matthew, C. K.; Ahern, K. G.; Van Holde, K. E. *Biochemistry*, 3rd ed.; Pearson Educacion: Madrid, 2002.

(2) Ying, W. *Antioxid. Redox Signaling* **2008**, *10*, 179−206.

(3) Khan, J. A.; Forouhar, F.; Tao, X.; Tong, L. *Expert Opin. Ther. Targets* **2007**, *11*, 695−705.

(4) Hileman, E. O.; Liu, J.; Albitar, M.; Keating, M. J.; Huang, P. *Cancer Chemother. Pharm.* **2004**, *53*, 209−219.

(5) Weckbecker, A.; Gro, H.; Hummel, W. *Adv. Biochem. Eng./Biotechnol.* **2010**, *120*, 195−242.

(6) Held, M.; Schmid, A.; B., V. B. J.; Witholt, B. *Pure Appl. Chem.* **2000**, *72*, 1337−1343.

(7) Chen, Q.; Gao, K.; Duan, Y.; Ye, Z.; Shi, L.; Yang, Y.; Zhou, Y. *J. Am. Chem. Soc.* **2012**, *134*, 2442−2448.

(8) Dibenedetto, A.; Stufano, P.; Macyk, W.; Baran, T.; Fragale, C.; Costa, M.; Aresta, M. *ChemSusChem* **2012**, *5*, 373−378.

(9) Kim, Y. H.; Yoo, Y. J. *Enzyme Microb. Technol.* **2009**, *44*, 129−134.

(10) Maenaka, Y.; Suenobu, T.; Fukuzumi, S. *J. Am. Chem. Soc.* **2012**, *134*, 367−374.

(11) Romain, C.; Gaillard, S.; Elmkaddem, M. K.; Toupet, L. c.; Fischmeister, C. d.; Thomas, C. M.; Renaud, J.-L. *Organometallics* **2010**, *29*, 1992−1995.

(12) Carrión, M. C.; Sepúlveda, F.; Jalón, F. l. a.; Manzano, B. R.; Rodríguez, A. M. *Organometallics* **2009**, *28*, 3822−3833.

(13) Wolfson, A.; Dlugy, C.; Shotland, Y.; Tavor, D. *Tetrahedron Lett.* **2009**, *50*, 5951−5953.

(14) Grau, M. M.; Poizat, M.; Arends, I. W. C. E.; Hollmann, F. *Appl. Organomet. Chem.* **2010**, *24*, 380−385.
(15) Matharu, D. S.; Morris, D. J.; Clarkson, G. J.; Wills, M. *Chem. Commun.* **2006**, 3232−3234.
(16) Noyori, R. *Angew. Chem., Int. Ed.* **2002**, *41*, 2008−2022.
(17) Fish, R. H. *Aust. J. Chem.* **2010**, *63*, 1505−1513.
(18) Leiva, C.; Lo, H. C.; Fish, R. H. *J. Organomet. Chem.* **2010**, *695*, 145−150.
(19) Tan, J.; Tang, W.; Sun, Y.; Jiang, Z.; Chen, F.; Xu, L.; Fan, Q.; Xiao, J. *Tetrahedron* **2011**, *67*, 6206−6213.
(20) Watanabe, M.; Kashiwame, Y.; Kuwata, S.; Ikariya, T. *Eur. J. Inorg. Chem.* **2012**, 504−511.
(21) Zhou, Z.; Ma, Q.; Zhang, A.; Wu, L. *Appl. Organomet. Chem.* **2011**, 556−561.
(22) Wang, C.; Villa-Marcos, B.; Xiao, J. *Chem. Commun.* **2011**, *47*, 9773−9785.
(23) Thai, T.; Therrien, B.; Süss-fink, G. *J. Organomet. Chem.* **2009**, *694*, 3973−3981.
(24) Sandoval, C. A.; Bie, F.; Matsuoka, A.; Yamaguchi, Y.; Naka, H.; Li, Y.; Kato, K.; Utsumi, N.; Tsutsumi, K.; Ohkuma, T.; Murata, K.; Noyori, R. *Chem. Asian J.* **2010**, *5*, 806−816.
(25) Creutz, C.; Chou, M. H. *J. Am. Chem. Soc.* **2009**, *131*, 2794−2795.
(26) Robertson, A.; Matsumoto, T.; Ogo, S. *Dalton Trans.* **2011**, *40*, 10304−10310.
(27) Martins, J. E. D.; Clarkson, G. J.; Wills, M. *Org. Lett.* **2009**, *11*, 847−850.
(28) Li, X.; Li, L.; Tang, Y.; Zhong, L.; Cun, L.; Zhu, J.; Liao, J.; Deng, J. *J. Org. Chem.* **2010**, *75*, 2981−2988.
(29) Wu, J.; Wang, F.; Ma, Y.; Cui, X.; Cun, L.; Zhu, J. *Chem. Commun.* **2006**, 1766−1768.
(30) Zhou, Z.; Ma, Q.; Sun, Y.; Zhang, A. *Heteroat. Chem.* **2010**, *21*, 505−514.
(31) Yan, Y. K.; Melchart, M.; Habtemariam, A.; Peacock, A. F.; Sadler, P. J. *J. Biol. Inorg. Chem.* **2006**, *11*, 483−488.
(32) Ruppert, R.; Herrmann, S.; Steckhan, E. *Chem. Commun.* **1988**, *1*, 1150−1151.
(33) Lo, H. C.; Leiva, C.; Buriez, O.; Kerr, J. B.; Olmstead, M. M.; Fish, R. H. *Inorg. Chem.* **2001**, *40*, 6705−6716.
(34) Habtemariam, A.; Melchart, M.; Fernandez, R.; Parsons, S.; Oswald, I. D. H.; Parkin, A.; Fabbiani, F. P.; Davidson, J. E.; Dawson, A.; Aird, R. E.; Jodrell, D. I.; Sadler, P. J. *J. Med. Chem.* **2006**, *49*, 6858−6668.
(35) Sheldrick, G. M. *SHELXL97*; University of Gottingen: Gottingen, Germany, 1997.
(36) Sheldrick, G. M. *Acta Crystallogr. A* **2007**, *64*, 112−122.
(37) Neese, F. *WIREs Comput. Mol. Sci.* **2012**, *2*, 73−78.
(38) Schäfer, A.; Horn, H.; Ahlrichs, R. *J. Chem. Phys.* **1992**, *97*, 2571−2577.
(39) Weigend, F.; Ahlrichs, R. *Phys. Chem. Chem. Phys.* **2005**, *7*, 3297−3305.
(40) Sinnecker, S.; Rajendran, A.; Klamt, A.; Diedenhofen, M.; Neese, F. *J. Phys. Chem. A* **2006**, *110*, 2235−2245.
(41) Grimme, S.; Antony, J.; Ehrlich, S.; Krieg, H.; Grimme, S.; Antony, J.; Ehrlich, S.; Krieg, H. *J. Chem. Phys.* **2010**, *132*, 154104−154117.
(42) Morris, R. E.; Aird, R. E.; Murdoch, S.; Chen, H.; Cummings, J.; Hughes, N. D.; Parsons, S.; Parkin, A.; Boyd, G.; Jodrell, D. I.; Sadler, P. J. *J. Med. Chem.* **2001**, *6*, 3616−3621.
(43) Peacock, A. F. A.; Habtemariam, A.; Fernández, R.; Walland, V.; Fabbiani, F. P. A.; Parsons, S.; Aird, R. E.; Duncan, I.; Sadler, P. J. *J. Am. Chem. Soc.* **2006**, *128*, 1739−1748.
(44) Canivet, J.; Süss-Fink, G.; Štěpnička, P. *Eur. J. Inorg. Chem.* **2007**, 4736−4742.
(45) Haquette, P.; Talbi, B.; Barilleau, L.; Madern, N.; Fosse, C.; Salmain, M. *Org. Biomol. Chem.* **2011**, *9*, 5720−5727.
(46) Wu, X.; Liu, J.; Li, X.; Zanotti-Gerosa, A.; Hancock, F.; Vinci, D.; Ruan, J.; Xiao, J. *Angew. Chem., Int. Ed* **2006**, *45*, 6718−6722.
(47) Wang, F.; Habtemariam, A.; van der Geer, E. P. L.; Fernández, R.; Melchart, M.; Deeth, R. J.; Aird, R.; Guichard, S.; Fabbiani, F. P.; Lozano-Casal, P.; Oswald, I. D. H.; Jodrell, D. I.; Parsons, S.; Sadler, P. J. *Proc. Natl. Acad. Sci. U. S. A.* **2005**, *102*, 18269−18274.
(48) Clayden, J.; Greeves, N.; Warren, S.; Wothers, P. *Organic Chemistry*, 1 ed.; Oxford University Press: Oxford, 2001.